ACADEMIC PRESS

Available online at www.sciencedirect.com

SCIENCE DIRECT®

Journal of Sound and Vibration 266 (2003) 369–387

JOURNAL OF SOUND AND VIBRATION

www.elsevier.com/locate/jsvi

Friction-induced sliding instability in a multi-degree-of-freedom system with oscillatory normal forces

E.J. Berger*, C.M. Krousgrill, F. Sadeghi

School of Mechanical Engineering, Purdue University, West Lafayette, IN 47907, USA

Received 30 October 1995; accepted 25 October 1996

Abstract

A multi-degree-of-freedom (m.d.o.f.) system excited by a rough moving surface has been developed to study friction-induced oscillations. The normal degrees of freedom allow for oscillatory normal forces, while the normal–tangential coupling of friction produces parametric excitation in the slipping equations of motion. After a modal change of variables, first order averaging has been used to produce a set of autonomous equations of motion. Eigenvalue analysis of the averaged equations has produced stability predictions for the steady sliding position. Numerical integration of the original system of equations has verified the existence of locally unstable oscillations for a system excited by a rough surface input. The combination of velocity-dependent friction and a harmonically varying normal force have been shown to produce large-amplitude oscillations, in some cases leading to stick–slip responses.

1. Introduction

The role of friction in the contact of mechanical components presents a problem of great interest and importance. The consequences of friction between two elastic bodies in sliding contact may be desirable, as in the stopping power of automobile brakes, or undesirable, as in the audible noise of brake squeal. Friction-excited oscillations are the usually undesirable result of the combination of friction behavior at the contact of two elastic bodies and overall system dynamics. Characterizing the relationship between the generally non-linear friction–velocity relationship and the dynamics of a particular contacting pair is paramount to understanding problems such as automatic transmission wet clutch engagement. Many researchers have studied friction-excited oscillations, concentrating on different aspects of the problem.

*Corresponding author. Structural Dynamics Lab., University of Cincinnati, P.O. Box 210072, Cincinnati, OH 45221-0072, USA.

E-mail address: ed.berger@uc.edu (E.J. Berger).

0022-460X/$ - see front matter © 2003 Elsevier Ltd. All rights reserved.
doi:10.1016/S0022-460X(03)00609-6

Of particular importance in the study of friction-excited oscillations is the variation of contact force. The problem was first examined critically by Tolstoi [1], who constructed a low speed friction apparatus to determine the influence of the normal degree of freedom (d.o.f.) on friction. He experimentally observed a friction force reduction when the normal d.o.f. resonance was excited. This resonant reduction in friction was attributed to the difference in mean separation of the bodies for the resonant and non-resonant cases. Godfrey [2] also recognized the interaction between system dynamics and friction by experimentally examining the influence of vibration between sliding components. Further discussion of mean separation and the real area of contact was seen in Budanov et al. [3]. They concluded that higher sliding velocities produced more violent asperity collisions and therefore a larger separation of the bodies. Rice and Ruina [4] used a state-dependent friction law and examined sliding stability. They determined the critical system stiffness value for stable sliding.

More recently, Hess and Soom [5,6] studied the interaction between friction and vibration. They predicted stability of steady sliding in a friction-excited system and augmented the Greenwood and Williamson [7] model for elastic contact with the rotation degree of freedom. Normal-angular coupling was also studied by Martins et al. [8], and later extended by Tworzydlo et al. [9]. In both works, a power law was used to model the constitutive behavior at a sliding contact interface. These works consider the kinematic coupling of the normal and angular modes, a phenomenon not unlike that observed in the study of brake squeal by Earles and Lee [10], among others. De-stabilizing effects in these models manifest themselves as non-symmetric (i.e., non-conservative) stiffness terms, possibly resulting in either flutter or divergence instabilities of linearized equations.

In this work, a new mechanism of instability has been investigated. Arising in systems with non-constant normal forces and velocity-dependent friction coefficient, the instability is the result of dynamic coupling of the tangential and normal modes of the slider. While many studies have focused on the friction-excited oscillations associated with a negative friction curve slope, the present work considers a friction-related steady sliding instability in a multiple-d.o.f. system possessing a friction law not restricted to negative slope. Due to the interaction of the oscillating normal force and the non-zero slope of the friction curve, a parametric damping term arises in the slipping equations of motion. This parametric excitation gives rise to combination resonances the stability of which have been determined using the first order averaging method of Krylov and Boguliubov [11]. The stability criterion developed for the combination resonance relates system damping to friction characteristics, normal force variations, and frequency tuning. The relationship between forcing frequency and system natural frequencies is critical. Unstable oscillations for the combination resonance are not excited by the negative damping-type instability of a negative friction curve slope. Rather, they are related to the magnitude of the friction curve slope and the tuning relationship of the forcing and natural frequencies.

2. Mathematical model and problem statement

The idealized system model is shown schematically in Fig. 1. Composed of m, 2-d.o.f. contact subsystems and one slider to which the contact subsystems are attached, the system has a total of $2m + 1$-d.o.f.s. Each contact subsystem is excited in the normal direction by a rough surface translating below, while the tangential d.o.f. is excited due to the normal–tangential coupling of

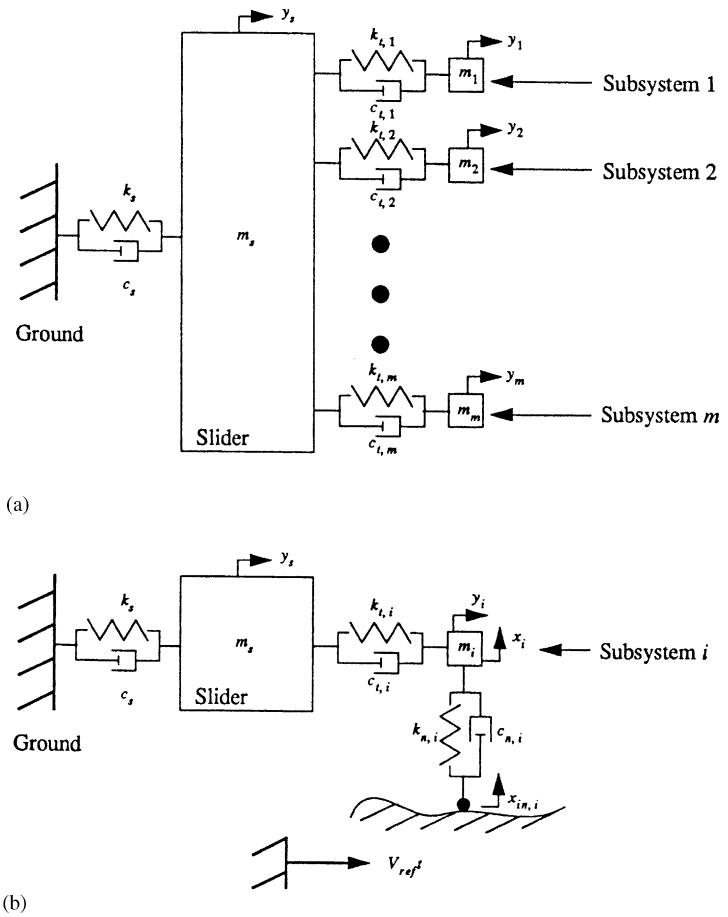

Fig. 1. A system schematic: (a) top view; (b) side view.

friction. The more massive slider, conversely, possesses a single tangential d.o.f., and it is coupled to each subsystem via a spring and dashpot. Therefore, the massive slider represents the large-scale motion of an elastic body in contact with a moving rough surface. The small subsystems represent the contact dynamics on a micro-scale; i.e., the subsystems model the contact of the elastic body and the moving surface on an asperity scale. The contact subsystems each have the potential for sticking, while the slider continuously slips. The rough surface input to each subsystem is independent; consequently, sticking of each contact subsystems occurs independently of the other subsystems.

Because of the piecewise description of the motion (i.e., sticking and slipping), the mathematical model is also developed piecewise. Consider the normal motion of one of the subsystems, say subsystem i, due to the rough surface moving below. The normal motion governing equation for the ith generalized co-ordinate is

$$m_i\ddot{x}_i + c_{n,i}(\dot{x}_i - \dot{x}_{in,i}) + k_{n,i}(x_i - x_{in,i}) = 0, \tag{1}$$

where i indicates the d.o.f. and n indicates that these are the normal d.o.f. stiffness and damping parameters. x_{in} and $\dot{x}_{in}$ are the input displacement and velocity, respectively, for the ith d.o.f.

The normal contact equations have been modelled using linear stiffness and damping elements in preparation for a stability analysis of the steady sliding solution later in the paper. It will be shown later that small, steady state normal oscillations drive the sliding instability for this system. Therefore, a linear approximation for the normal contact governing equations will not invalidate the conclusions of the stability analysis, and is the starting point for the normal contact model.

The slipping equation of motion for the ith tangential response co-ordinate is

$$m_i\ddot{y}_i + c_{t,i}\dot{y}_i + k_{t,i}y_i = F_{f,i} + c_{t,i}\dot{y}_s + k_{t,i}y_s, \tag{2}$$

where

$$F_{f,i}(t) = \mu_i(V_{rel,i})|N_i(t)|\,\mathrm{sgn}(V_{rel,i}), \tag{3}$$

and where the subscript t indicates that these stiffness and damping parameters are for tangential motion. μ_i is the coefficient of friction for the ith d.o.f. and N_i is the normal force for the ith d.o.f. y_s is the displacement of the slider, while y_i is the tangential displacement of the ith subsystem. The normal force is time-dependent and composed of two parts; one part is the static (constant) normal force, denoted by $N_{o,i}$, while the other is the normal force fluctuations due to normal response, denoted by $m_i\ddot{x}_i$:

$$N_i(t) = N_{o,i} + m_i\ddot{x}_i. \tag{4}$$

The time dependence of the normal force is the result of a normal direction oscillatory response, x_i.

The friction model under slipping conditions can then be described as follows. The friction coefficient $\mu_i(V_{rel,i})$ is a function of sliding velocity, thus capturing the well-documented variation of friction with relative velocity. The normal force is a function of time, resulting from normal oscillations in the subsystems. The friction force, therefore, is a function of both sliding velocity and normal motion, as described in Eq. (3).

Tangential motion during sticking for the ith d.o.f. is prescribed as

$$\dot{y}_i = V_{ref,i}, \quad \ddot{y}_i = 0, \tag{5}$$

where $V_{ref,i}$ is the (reference) velocity of the surface moving beneath the ith contact subsystem.

Next, consider the slider to which the 2-d.o.f. contact subsystems are attached. The slider is considered to have only tangential motion. It is excited only by its coupling to the subsystems, and it is attached to global ground via a spring and dashpot. The equation of motion for the slider is

$$m_s\ddot{y}_s + c_s\dot{y}_s + k_s y_s = \sum_{i=1}^{i=m} F_i, \tag{6}$$

where F_i is the reaction force developed in the ith subsystem spring and dashpot. The matrix slipping equation of motion can then be assembled:

$$\mathbf{M}\{\ddot{Q}\} + \mathbf{C}\{\dot{Q}\} + \mathbf{K}\{Q\} = \mathbf{F}, \tag{7}$$

where $\{Q\}$ is given as

$$\{Q\} = [y_s y_1 \cdots y_m x_1 \cdots x_m]^{\mathrm{T}}, \tag{8}$$

and **M**, **C** and **K** have the following forms:

$$\mathbf{M} = \begin{bmatrix} m_s & 0 & \cdots & 0 & 0 & \cdots & 0 \\ 0 & m_1 & \cdots & 0 & 0 & \cdots & 0 \\ 0 & 0 & \ddots & 0 & 0 & \cdots & 0 \\ 0 & 0 & \cdots & m_m & 0 & \cdots & 0 \\ 0 & 0 & \cdots & 0 & m_1 & \cdots & 0 \\ 0 & 0 & \cdots & 0 & 0 & \ddots & 0 \\ 0 & 0 & \cdots & 0 & 0 & \cdots & m_m \end{bmatrix}, \tag{9}$$

$$\mathbf{K} = \begin{bmatrix} k_s + \sum_{i=1}^{i=m} k_{t,i} & -k_{t,1} & \cdots & -k_{t,m} & 0 & \cdots & 0 \\ -k_{t,1} & k_{t,1} & \cdots & 0 & 0 & \cdots & 0 \\ \vdots & 0 & \ddots & 0 & 0 & \cdots & 0 \\ -k_{t,m} & 0 & \cdots & k_{t,m} & 0 & \cdots & 0 \\ 0 & 0 & \cdots & 0 & k_{n,1} & \cdots & 0 \\ \vdots & 0 & \cdots & 0 & 0 & \ddots & 0 \\ 0 & 0 & \cdots & 0 & 0 & \cdots & k_{n,m} \end{bmatrix}. \tag{10}$$

C has the same form as **K**. **F** is defined as

$$\mathbf{F} = [0 \;\; F_{f,1} \;\; \cdots \;\; F_{f,m} \;\; 0 \;\; \cdots \;\; 0]^{\mathrm{T}}. \tag{11}$$

Normal excitation to the system is provided by the rough surface translating beneath the contact subsystems. In order to investigate roughness-related phenomena, a sinusoidal profile with characteristic height $h_{asp,i}$ is used:

$$x_{in,i} = h_{asp,i} \sin\left(\frac{2\pi X_i}{\lambda_i}\right), \tag{12}$$

where X_i is the distance travelled and λ_i is the wavelength of the surface beneath the ith d.o.f. X_i includes one component due to the motion of the surface itself and one component due to the tangential response of the subsystem.

In the zero surface roughness case, the normal force is constant, and the steady sliding friction force for the ith d.o.f. is

$$F_{f,i,ss} = \mu(V_{ref,i})N_{o,i}. \tag{13}$$

It is assumed that for the small surface roughness features, the long time solution of Eq. (7) in the phase space consists not of discrete points, but of small closed trajectories, representing periodic motion. The stability of these periodic solutions is investigated, and conditions for the existence of parametric instabilities are derived in terms of friction curve slope at the steady sliding position.

3. Linearized equations of motion

The goal of this analysis is to determine the stability of the long time solution to the system of equations (7). For small roughness features (i.e., small $h_{asp,i}$), the oscillatory part of the normal force, Eq. (4), is small, and the long time solution to Eq. (7) involves small, periodic, non-sticking solutions (small, closed trajectories in the phase space). If the trajectories are small, then as a first approximation, the small tangential response is neglected when calculating X_i. Therefore,

$$X_i \approx V_{ref,i}t, \tag{14}$$

and the rough surface input to the ith co-ordinate becomes an explicit function of time:

$$x_{in,i} = h_{asp,i}\sin(\omega_{o,i}t), \tag{15}$$

where

$$\omega_{o,i} = \frac{2\pi V_{ref,i}}{\lambda_i}. \tag{16}$$

The normal direction input no longer relies upon the tangential direction response. This decoupling allows for explicit solution for the displacement variables corresponding to the normal response co-ordinates. The steady state normal response for the ith d.o.f. is

$$x_i(t) = M_i\cos(\omega_{o,i}t - \phi_i). \tag{17}$$

In Eq. (17),

$$M_i = h_{asp,i}\left[\frac{k_{n,i}^2 + (c_{n,i}\omega_{o,i})^2}{(k_{n,i} - m_i\omega_{o,i}^2)^2 + (c_{n,i}\omega_{o,i})^2}\right]^{1/2}, \tag{18}$$

$$\phi_i = \tan^{-1}\left[\frac{c_{n,i}\omega_{o,i}}{k_{n,i} - m_i\omega_{o,i}^2}\right] - \tan^{-1}\left[\frac{k_{n,i}}{c_{n,i}\omega_{o,i}}\right]. \tag{19}$$

The remaining variables are contained in the vector $\{\hat{Q}\}$:

$$\{\hat{Q}\} = [y_s \;\; y_1, \;\; \cdots \;\; y_m]^{\mathrm{T}}, \tag{20}$$

which has been reduced to only $m+1$ unknowns.

Using the steady state solution (17) in the friction force equation (3), the non-linear friction force for the ith response co-ordinate is written as

$$F_{f,i} = \mu_i(V_{rel,i})[N_{o,i} - m_i M_i\omega_{o,i}^2\cos(\omega_{o,i}t - \phi_i)]. \tag{21}$$

Note that sgn $(V_{rel,i})$ has been dropped because continuous sliding is assumed to occur for small oscillations about the steady sliding position.

In order to investigate the stability of periodic solutions to the decoupled equations, the friction force is linearized using a Taylor series expansion about the steady sliding position:

$$\mu_i = \mu_i^* + S_i\dot{y}_i + \cdots, \tag{22}$$

where

$$\mu_i^* = \mu_i(V_{ref,i}), \quad S_i = \left.\frac{\mathrm{d}\mu}{\mathrm{d}V_{rel}}\right|_{V_{rel}=V_{ref}}. \tag{23, 24}$$

It is assumed that the same friction–velocity relation describes the contact of each subsystem, although the contacting velocities $V_{ref,i}$ of the subsystems are independent. Using the linearized friction coefficient (22), the linearized friction force becomes

$$F_{f,i} = \Delta_i + \delta_i + \beta_i \cos(\omega_{o,i}t - \phi_i) + \gamma_i \cos(\omega_{o,i}t - \phi_i)\dot{y}_i, \tag{25}$$

where

$$\Delta_i = \mu_i^* N_{o,i}, \quad \delta_i = S_i N_{o,i}, \quad \beta_i = -M_i\omega_{o,i}^2\mu_i^*, \quad \gamma_i = -M_i\omega_{o,i}^2 S_i. \tag{26}$$

Using the modal transformation

$$\{\hat{Q}\} = \hat{\mathbf{R}}\{z\}, \tag{27}$$

where $\hat{\mathbf{R}}$ is the mass-normalized matrix of eigenvectors, yields the system equations of motion

$$\mathbf{I}\{\ddot{\eta}\} + [[\xi] - \mathbf{\Gamma}(t)]\{\dot{\eta}\} + \mathbf{\Omega}_n^2\{\eta\} = \{\hat{\beta}\}, \tag{28}$$

where

$$\{\eta\} = \{z\} - [\Omega_n^2]^{-1}\{\hat{\Delta}\}, \quad \{\hat{\Delta}\} = \hat{\mathbf{R}}^{\mathrm{T}}[0 \;\; \Delta_1 \;\; \cdots \;\; \Delta_m]^{\mathrm{T}},$$

$$\mathbf{\Gamma}(t) = \hat{\mathbf{R}}^{\mathrm{T}}\begin{bmatrix} 0 & 0 & \cdots & 0 \\ 0 & \gamma_1\cos(\omega_{o,1}t - \phi_1) & \cdots & 0 \\ 0 & 0 & \ddots & 0 \\ 0 & 0 & \cdots & \gamma_m\cos(\omega_{o,m}t - \phi_m) \end{bmatrix}\hat{\mathbf{R}}, \tag{29}$$

$$[\xi] = \hat{\mathbf{R}}^{\mathrm{T}}\left\{[C] + \begin{bmatrix} 0 & 0 & \cdots & 0 \\ 0 & \delta_1 & \cdots & 0 \\ 0 & 0 & \ddots & 0 \\ 0 & 0 & \cdots & \delta_m \end{bmatrix}\right\}\hat{\mathbf{R}},$$

$$\{\hat{\beta}\} = \hat{\mathbf{R}}^{\mathrm{T}}[0 \;\; \beta_1\cos(\omega_{o,1}t - \phi_1) \;\; \cdots \;\; \beta_m\cos(\omega_{o,m}t - \phi_m)]^{\mathrm{T}}.$$

The explicit form of the inhomogeneous forcing for the ith co-ordinate is

$$\hat{\beta}_i = \sum_{j=1}^{j=m+1} \hat{R}_{ji}\beta_j \cos(\omega_{o,j}t - \phi_j), \tag{30}$$

where $\hat{R}_{ji}$ are the entries in the modal matrix $\hat{\mathbf{R}}$. As is revealed by Eq. (30), $\hat{\beta}_i$ contains terms with the forcing frequencies of each subsystem due to modal coupling.

4. Stability analysis

Small physical damping has been assumed in the analysis. Furthermore, according to Eq. (26), the two friction-related damping terms, δ_i and γ_i, are both proportional to the *slope* of the friction

curve S_i. Conversely, the forcing parameter β_i is scaled by the steady sliding friction coefficient μ_i^*. If it is assumed that the linearized slope of the friction curve S_i is of the same order as the light damping, it is logical to scale the following parameters as

$$[\xi] = \varepsilon[\hat{\xi}], \quad \mathbf{\Gamma} = \varepsilon\hat{\mathbf{\Gamma}}, \quad 0 < \varepsilon \ll 1. \tag{31}$$

However, it is *not* assumed that the steady sliding friction coefficients μ_i^* are small; hence the inhomogeneous forcing terms are *not* rescaled by ε.

Eq. (28) is now rewritten as

$$\mathbf{I}\{\ddot{\eta}\} + \varepsilon[[\hat{\xi}] - \hat{\mathbf{\Gamma}}(\mathbf{t})]\{\dot{\eta}\} + \mathbf{\Omega}_n^2\{\eta\} = \{\hat{\beta}\}. \tag{32}$$

The Cartesian transformation $(\eta, \dot{\eta}) \rightarrow (\mathbf{A}, \mathbf{B})$ is used to express the $\varepsilon = 0$ solution to system (32):

$$\eta_i(t) = A_i \cos(\Omega_i t) + B_i \sin(\Omega_i t) + \sum_{j=1}^{j=m+1} F_{ij} \cos(\omega_{o,j} t - \phi_j), \tag{33}$$

$$\dot{\eta}(t) = -A_i \Omega_i \sin(\Omega_i t) + B_i \Omega_i \cos(\Omega_i t) - \sum_{j=1}^{j=m+1} F_{ij} \omega_{o,j} \sin(\omega_{o,j} t - \phi_j), \tag{34}$$

where

$$F_{ij} = \frac{R_{ji}\beta_j}{\Omega_i^2 - \omega_{o,j}^2}. \tag{35}$$

The resulting set of $2m + 2$ first order differential equations is

$$\dot{A}_i = \frac{\varepsilon}{\Omega_i} \sin(\Omega_i t) f_i(\mathbf{A}, \mathbf{B}, t), \quad \dot{B}_i = -\frac{\varepsilon}{\Omega_i} \cos(\Omega_i t) f_i(\mathbf{A}, \mathbf{B}, t). \tag{36, 37}$$

In Eqs. (36) and (37), the non-autonomous function f_i is

$$f_i = \sum_{j=1}^{j=m+1} \left\{ \left[\xi_{ij} - \sum_{k=1}^{k=m+1} \Gamma_{ij} \cos(\omega_{o,k} t - \phi_k) \right] \times \left[-A_j \Omega_j \sin(\Omega_j t) + B_j \Omega_j \cos(\Omega_j t) + \sum_{k=1}^{k=m+1} -F_{ik} \omega_{o,k} \sin(\omega_{o,k} t - \phi_k) \right] \right\}. \tag{38}$$

Using definition (38), the first order Eqs. (36) and (37) are expanded in Fourier series in order to reveal the resonance frequencies of the system. These non-autonomous equations contain terms the circular frequencies of which are sums and differences of all the systems natural frequencies Ω_i and forcing frequencies $\omega_{o,i}$. These time-dependent equations will be reduced to autonomous equations via first order averaging. The averaging operator of Krylov and Boguliubov [11] is given by

$$A\{\cdots\} = \lim_{T \to \infty} \frac{1}{T} \int_0^T \{\cdots\} \, \mathrm{d}t. \tag{39}$$

The averaging operator is applied termwise to the first order Eqs. (36) and (37); the surviving terms are those which are constant and those with circular frequencies nearly equal to zero. The resulting averaged (autonomous) equations contain the critical information for stability

prediction. Each of the resonance conditions is examined individually below. In the subsequent analysis, it is assumed that the system natural frequencies are distinct, thus precluding the existence of the $i-j$ internal resonance.

4.1. Case I: $\Omega_i \approx \omega_{o,j}$

In this case, the averaged equations are

$$\begin{Bmatrix} \dot{A}_i \\ \dot{B}_i \end{Bmatrix} = \frac{1}{2}\varepsilon \begin{bmatrix} -\xi_{ii} & 2\sigma \\ -2\sigma & -\xi_{ii} \end{bmatrix} \begin{Bmatrix} A_i \\ B_i \end{Bmatrix} + \varepsilon \begin{Bmatrix} \dfrac{-F_{ij}\omega_{o,j}\xi_{ii}}{2}\cos(-\phi_j) + F_{ij}\sigma \sin(-\phi_j) \\ \dfrac{-F_{ij}\omega_{o,j}\xi_{ii}}{2}\sin(-\phi_j) + F_{ij}\sigma \cos(-\phi_j) \end{Bmatrix}, \tag{40}$$

where σ is the detuning parameter:

$$\omega_{o,j} = \Omega_i + \varepsilon\sigma. \tag{41}$$

The eigenvalues of the coefficient matrix in Eq. (40) are

$$\lambda_{1,2} = -\xi_{ii} \mp \mathrm{i}(4\sigma), \tag{42}$$

indicating a stable periodic solution $\eta_i(t)$ as long as the effective modal damping ξ_{ii} is positive.

4.2. Case II: $\Omega_i \pm \Omega_j \approx \omega_{o,k}$

After detuning according to

$$\omega_{o,k} = \Omega_i + \Omega_j + \varepsilon\sigma, \tag{43}$$

the averaged equations are

$$\begin{Bmatrix} \dot{A}_i \\ \dot{B}_i \\ \dot{A}_j \\ \dot{B}_j \end{Bmatrix} = \varepsilon \begin{bmatrix} \dfrac{\xi_{ii}}{2} & -\sigma & \dfrac{-\gamma_{ij}\Omega_j}{4(\omega_{o,k}-\Omega_j)}C & \dfrac{\gamma_{ij}\Omega_j}{4(\omega_{o,k}-\Omega_j)}S \\ \sigma & \dfrac{-\xi_{ii}}{2} & \dfrac{\gamma_{ij}\Omega_j}{4(\omega_{o,k}-\Omega_j)}S & \dfrac{\gamma_{ij}\Omega_j}{4(\omega_{o,k}-\Omega_j)}C \\ \dfrac{-\gamma_{ij}(\omega_{o,k}-\Omega_j)}{4\Omega_j}C & \dfrac{\gamma_{ij}(\omega_{o,k}-\Omega_j)}{4\Omega_j}S & \dfrac{\xi_{jj}}{2} & 0 \\ \dfrac{-\gamma_{ij}(\omega_{o,k}-\Omega_j)}{4\Omega_j}S & \dfrac{\gamma_{ij}(\omega_{o,k}-\Omega_j)}{4\Omega_j}C & 0 & \dfrac{\xi_{jj}}{2} \end{bmatrix} \times \begin{Bmatrix} A_i \\ B_i \\ A_j \\ B_j \end{Bmatrix}, \tag{44}$$

where

$$C = \cos(-\phi_k), \quad S = \sin(-\phi_k). \tag{45,46}$$

The eigenvalues of the coefficient matrix in Eq. (44) are

$$\lambda_{1,2,3,4} = \frac{1}{4}\left[-(\xi_{ii}+\xi_{jj}) \pm 2\mathrm{i}\sigma \pm \sqrt{(\xi_{ii}-\xi_{jj})^2 + \Gamma_{ij}^2 - 4\sigma^2 + 4\mathrm{i}\sigma(\xi_{jj}-\xi_{ii})}\right]. \tag{47}$$

For eigenvalues with negative real parts, the critical value of modal parametric excitation is

$$\Gamma_{crit,ij} = 2\frac{\sqrt{\xi_{ii}\xi_{jj}}}{(\xi_{ii}+\xi_{jj})}\sqrt{(\xi_{ii}+\xi_{jj})^2 + 4\sigma^2}. \tag{48}$$

The averaged equations for the difference resonance case $\Omega_i - \Omega_j \approx \omega_{o,k}$ are obtained by changing the sign of Ω_j in Eq. (44). The stability prediction of Eq. (48) is precisely the same for the difference resonance case.

4.3. *Case* III: $\Omega_i \approx \omega_{o,j} \times \omega_{o,k}$

For the detuning

$$\omega_{o,j} + \omega_{o,k} = \Omega_i + \varepsilon\sigma, \tag{49}$$

the averaged equations are

$$\begin{Bmatrix} \dot{A}_i \\ \dot{B}_i \end{Bmatrix} = \varepsilon \begin{bmatrix} \dfrac{-\xi_{ii}}{2} & 2\sigma \\ -2\sigma & \dfrac{-\xi_{ii}}{2} \end{bmatrix} \begin{Bmatrix} A_i \\ B_i \end{Bmatrix} + \begin{Bmatrix} \dfrac{-F_{ik}\omega_{o,k}\Gamma_{ij}}{4}\cos(-\phi_j - \phi_k) \\ \dfrac{-F_{ik}\omega_{o,k}\Gamma_{ij}}{4}\sin(-\phi_j - \phi_k) \end{Bmatrix}. \tag{50}$$

The eigenvalues of the coefficient matrix are

$$\lambda_{1,2} = -\frac{\xi_{ii}}{2} \mp \mathrm{i}(2\sigma). \tag{51}$$

The linearized response is stable for positive effective modal damping ξ_{ii}. The results given are also applicable for the difference case $\Omega_i \approx \omega_{o,j} - \omega_{o,k}$.

4.4. *Non-resonant motion*

For the case of no special frequency relationships, the averaged equations are:

$$\begin{Bmatrix} \dot{A}_i \\ \dot{B}_i \end{Bmatrix} = \varepsilon \begin{bmatrix} \dfrac{-\xi_{ii}}{2} & 0 \\ 0 & \dfrac{-\xi_{ii}}{2} \end{bmatrix} \begin{Bmatrix} A_i \\ B_i \end{Bmatrix}, \tag{52}$$

which clearly indicates that for positive effective damping ξ_{ii} the linearized response is stable.

The stability conditions are summarized in Table 1; however, several points deserve further discussion. Consider the interesting case of internal combination resonance, Case II. Note that the stability boundary $\Gamma_{crit,ij}$ found in Eq. (47) forms a hyperbola in the (Γ_{ij}, σ)-parameter space which is symmetric with respect to the σ-axis. Recalling the definition of Γ_{ij}, Eq. (29), it is clear that for a negative slope of the friction curve, Γ_{ij} could be less than zero. The product of the velocity-dependent friction and a special frequency relationship, this *friction-related* instability relies upon the existence of a sufficiently large parametric excitation amplitude.

Table 1
Summary of stability criteria

Frequency relationship	Stability condition 1	Stability condition 2
Case I: $\Omega_i \approx \omega_{o,j}$	$\xi_{ii} > 0$	N/A
Case II: $\Omega_i \pm \Omega_j \approx \omega_{o,k}$	$\xi_{ii} > 0,\ \xi_{jj} > 0$	$\lvert\Gamma_{ij}\rvert < \lvert\Gamma_{crit,ij}\rvert$
Case III: $\Omega_i \approx \omega_{o,j} \pm \omega_{o,k}$	$\xi_{ii} > 0$	N/A
No special relationship	$\xi_{ii} > 0$	N/A

Before turning to numerical analysis to corroborate the linearized stability predictions and to investigate the global effects of local instabilities, it is instructive to discuss the relationships between the various system operating parameters. It is clear that increasing the system damping makes the effective damping ξ_{ij} larger. However, increasing the static part of the normal force $N_{o,i}$ plays two different roles depending upon the sign of the friction curve slope. For the positive slope case, increasing the static normal force has a stabilizing effect, while for the negative slope case, increasing the static normal force has a destabilizing effect. Larger slope magnitudes produce larger parametric excitation amplitudes, but depending upon the sign of the slope, they produce either more or less friction-related damping. The interaction of the various system parameters is quite complex; a numerical example reveals some of the subtlety.

5. Numerical results and discussion

In order to demonstrate the utility of the stability predictions developed above, the 3-d.o.f. system shown in Fig. 2 is examined. The system under consideration possesses two d.o.f.s in the transverse direction (y direction), one d.o.f. in the normal direction (x direction). The system is excited by the moving surface with sinusoidal roughness below it. The model allows for sticking of the contact subsystem, velocity-dependent friction, and oscillatory normal force due to the rough surface input, expressed as

$$x_{in}(\tau) = \sin(2\pi \hat{V}_{ref}\tau/\omega_1\hat{\lambda}), \tag{53}$$

where

$$\hat{V}_{ref} = V_{ref}/h_{asp}, \quad \hat{\lambda} = \lambda/h_{asp}.$$

Therefore, the normal motion for the decoupled system is governed by

$$x'' + \zeta_n x' + \omega_n^2 x = \zeta_n x'_{in} + \omega_n^2 x_{in}, \tag{54}$$

where

$$\zeta_n = \frac{c_n}{m_1\omega_1}, \quad \omega_n = \frac{1}{\omega_1}\sqrt{\frac{k_n}{m_1}}.$$

Solving for the normal response allows the linearized friction force to be written as follows:

$$F_f(V_{rel},\tau) = \mu(V_{rel})[\hat{N}_o - \bar{M}\omega_o^2\cos(\omega_r\tau - \phi)], \tag{55}$$

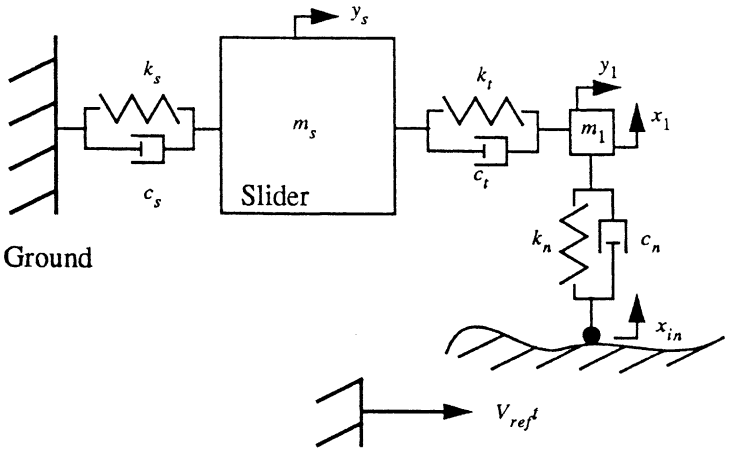

Fig. 2. The 3-d.o.f. system used for the numerical study.

where

$$\hat{N}_o = N_o/m_1\omega_1^2, \quad \bar{M} = M/m_1\omega_1^2, \quad \omega_r = \omega_o/\omega_1. \tag{56}$$

The dimensionless tangential equations of motion for the decoupled system are

$$\begin{bmatrix} 1 & 0 \\ 0 & \bar{m}_1 \end{bmatrix}\mathbf{y}'' + \zeta_1\begin{bmatrix} 1+\bar{c}_1 & -\bar{c}_1 \\ -\bar{c}_1 & \bar{c}_1 \end{bmatrix}\mathbf{y}' + \begin{bmatrix} 1+\bar{k}_1 & -\bar{k}_1 \\ -\bar{k}_1 & \bar{k}_1 \end{bmatrix}\mathbf{y} = \begin{Bmatrix} 0 \\ F_f(\tau) \end{Bmatrix}, \tag{57}$$

where

$$\bar{m}_1 = m_t/m_s, \quad \bar{c}_1 = c_t/c_s, \quad \bar{k}_1 = k_t/k_s, \quad \omega_1^2 = k_s/m_1, \tag{58}$$

$$\zeta_1 = \frac{c_t}{(m_1\omega_1)}, \quad \tau = \omega_1 t, \quad (\cdots)' = \mathrm{d}/\mathrm{d}\tau(\cdots).$$

The input parameters used for numerical study of the model and the stability predictions are given in Table 2.

The friction–velocity relation used in the simulations is shown in Fig. 3 and described mathematically by

$$\mu = \begin{cases} 0.75 - 0.03|V_{rel}|, & |V_{rel}| < 15.0, \\ 0.3, & |V_{rel}| \geqslant 15.0. \end{cases} \tag{59}$$

For the parameters used in this study, the effective modal damping ξ_{ij} is non-negative for all reference velocities. As a result, the negative slope of the friction curve is *insufficient* to produce the negative damping-type instabilities of Case I ($\Omega_i \approx \omega_{o,j}$), Case III ($\Omega_i \approx \omega_{o,j} \pm \omega_{o,k}$) and the non-resonant case. The numerical study will focus on the Case II ($\Omega_i \pm \Omega_j \approx \omega_{o,k}$) internal combination resonance.

Following the procedure outlined above, the normal response is decoupled from the tangential response, and the resulting 2-d.o.f. system has non-dimensional natural frequencies of

$$\Omega_1 = 0.9950, \quad \omega_2 = 31.7807. \tag{60}$$

Table 2
Input parameters

$\bar{m}_1 = 0.01$	$\hat{\lambda} = 16.67$
$\bar{k}_1 = 10.0$	$\omega = 1.0$
$\bar{c}_1 = 1.0$	$\zeta_1 = 0.015$
$\bar{k}_n = 0.1$	$\zeta_n = 0.1$
$\omega_n = \sqrt{10.0}$	$\hat{N}_o = 0.05$

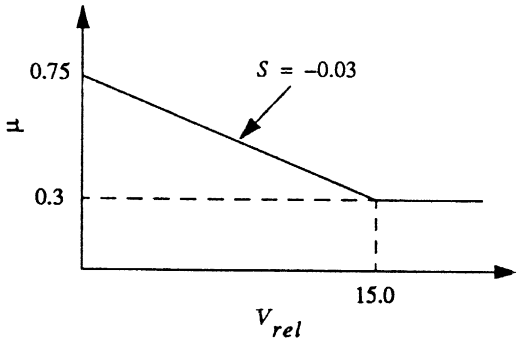

Fig. 3. The piecewise linear friction law.

The surface frequencies ω_o of interest are given by

$$\omega_o \approx 2\Omega_1 = 1.9900, \quad \omega_o \approx \Omega_2 - \Omega_1 = 30.7857, \quad \omega_o \approx \Omega_2 + \Omega_1 = 32.7757$$

and

$$\omega_o \approx 2\Omega_2 = 63.5614.$$

Linearized analysis in the neighborhood of each of these frequencies produces predictions concerning the stability of the steady sliding position as a function of forcing frequency (i.e., sliding speed). The stability map for the two combination resonances for the conditions listed in Table 2 is shown in Fig. 4. The frequency ranges producing unstable local responses are

$$\omega_o \approx \Omega_2 - \Omega_1 \quad \Rightarrow \quad 30.74 < \omega_o < 30.83.$$

$$\omega_o \approx \Omega_2 + \Omega_1 \quad \Rightarrow \quad 32.72 < \omega_o < 32.83,$$

$$\omega_o \approx 2\Omega_2 \quad \Rightarrow \quad 62.70 < \omega_o < 64.45.$$

Note that since Ω_1 is much smaller than Ω_2, the additive- and difference-type combination resonances occur at nearly the same frequency. As a result, the conclusions drawn about stable and unstable responses, and their impact on global system dynamics, are similar for both cases. Therefore, the results for the $\omega_o \approx \Omega_2 - \Omega_1$ difference combination resonance are presented. Also shown are the results for the $\omega_o \approx 2\Omega_2$ parametric resonance. The three non-linear, uncoupled equations of motion (54) and (57) have been integrated numerically, and the results are reported below.

Consider first the case of the difference-type combination resonance, $\omega_o \approx \Omega_2 - \Omega_1$. In Fig. 5, the stable response corresponding to $\omega_o = 30.16$ consists of small-amplitude periodic oscillations.

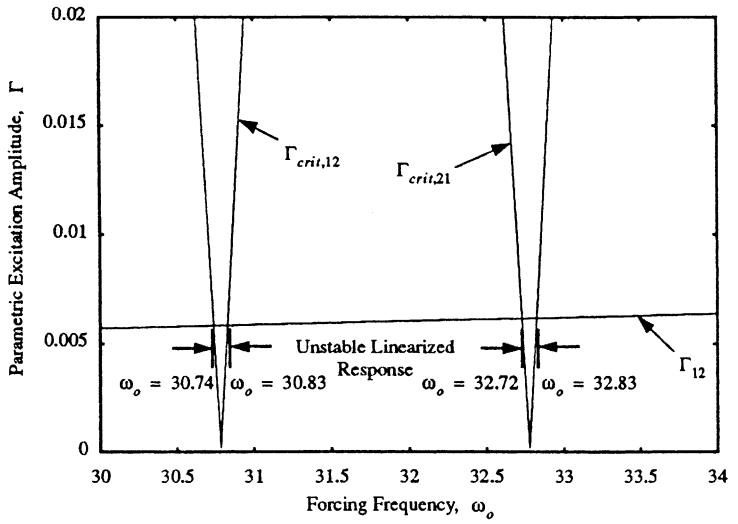

Fig. 4. The stability map for $\omega_o \approx \Omega_1 + \Omega_2$.

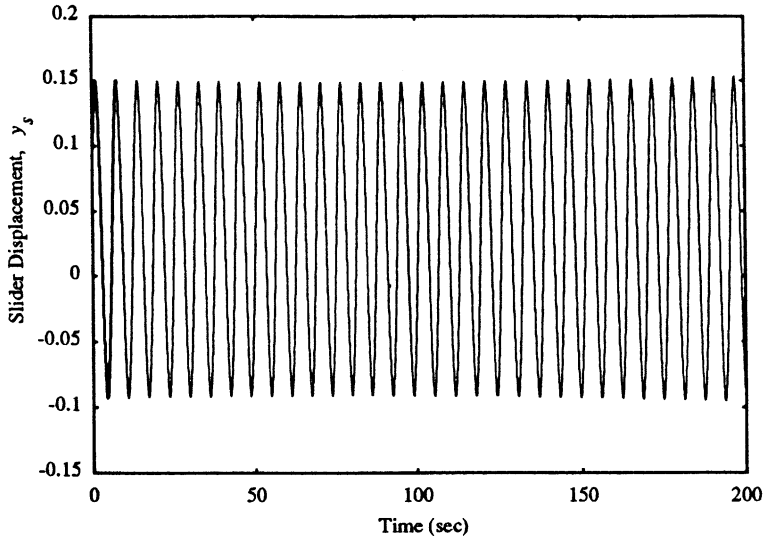

Fig. 5. The slider response for $\omega_o = 30.16$.

However, for the forcing frequency $\omega_o = 30.78$, the local response is unstable, and the oscillations grow slowly. The response contains three frequency components, the natural frequencies of the system and the forcing frequency. The amplitude envelope for these growing oscillations is shown in Fig. 6, with a close-up view shown in Fig. 7. The multi-frequency makeup of the response and its slow growth are evident in Fig. 7. In both cases $\omega_o = 30.16$ and $\omega_o = 30.78$, the system clearly has one dominant frequency, that being the first natural frequency $\Omega_1 = 0.9950$. Superimposed on this low frequency is a higher frequency component related to both the forcing frequency and the

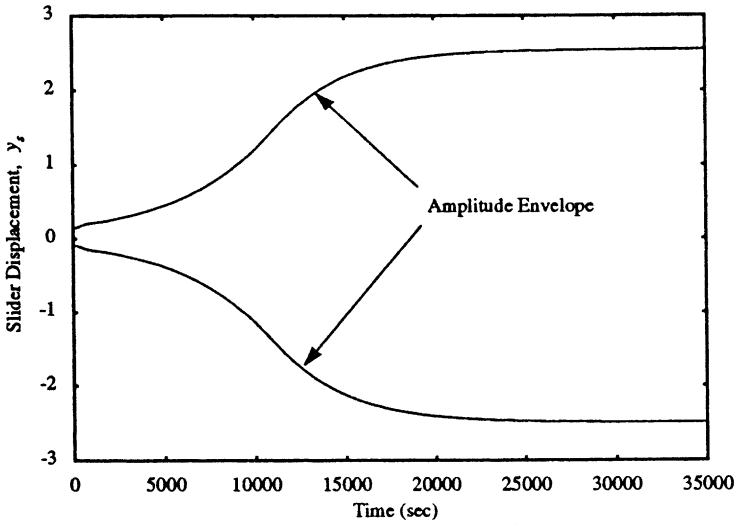

Fig. 6. The slider response envelope for $\omega_o = 30.78$.

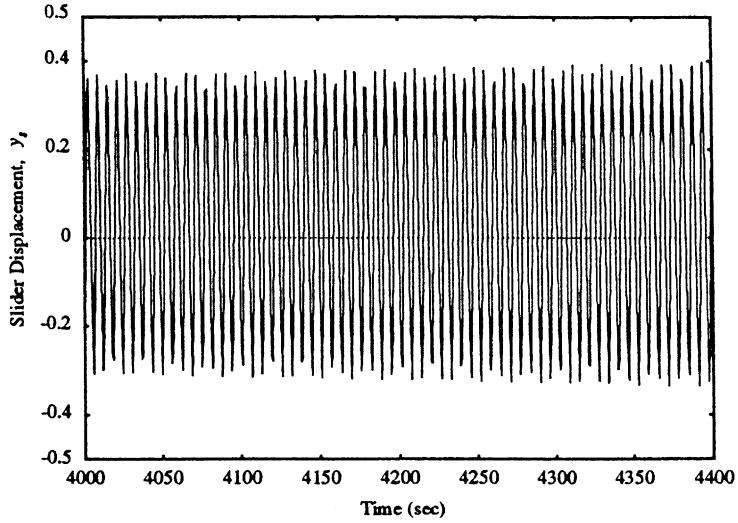

Fig. 7. A close-up of the slider time response for $\omega_o = 30.78$.

second natural frequency. For the two cases shown, the high-frequency component of the response shows a beating phenomenon, indicative of the slight frequency mistuning of the forcing frequency and second natural frequency. For the case $\omega_o = 30.78$, the amplitude of high-frequency oscillations is not significantly higher than that for the case $\omega_o = 30.16$. However, the frequency tuning is correct for the existence of the $\omega_o \approx \Omega_2 - \Omega_1$ combination resonance. The unstable oscillations result in a large-amplitude response, in this case leading to a steady state stick–slip response. The same phenomenon can be observed for the $\omega_o \approx \Omega_1 + \Omega_2$ additive combination resonance, for which an unstable local response is predicted for $32.72 < \omega_o < 32.83$.

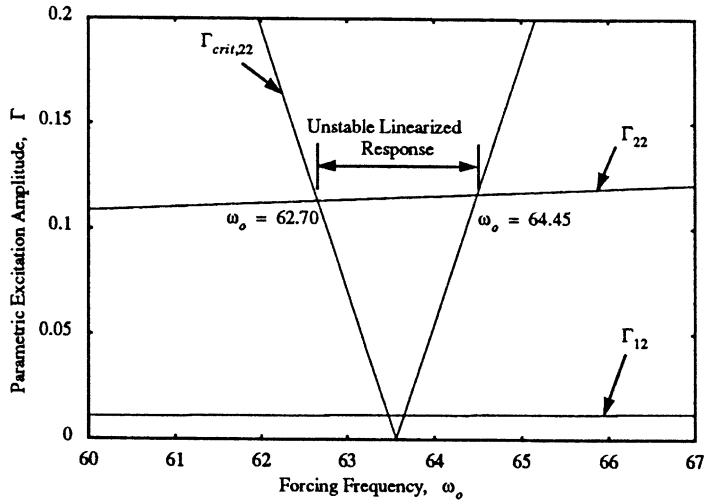

Fig. 8. The stability map for $\omega_o \approx 2\Omega_2$.

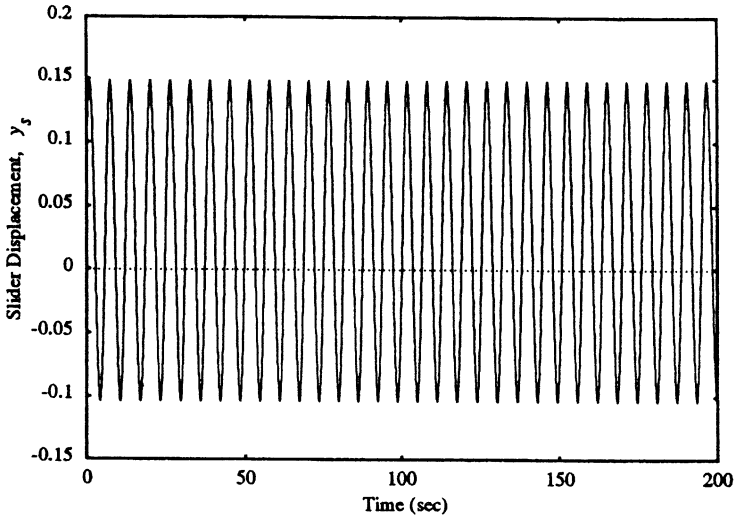

Fig. 9. The slider response for $\omega_o = 62.0$.

Fig. 8 shows the stability map for the case $\omega_o \approx 2\Omega_2$, clearly indicating an unstable local response for the frequency range $62.70 < \omega_o < 64.45$. Time histories for the non-linear decoupled equations with forcing frequencies in the stable and unstable regions are shown in Figs. 9–13. The stable, small-amplitude steady state response associated with the forcing frequency $\omega_o = 62.0$ is demonstrated in Fig. 9. Conversely, the unstable local response predicted for the forcing frequency $\omega_o = 63.5$ produces the small-amplitude response of Fig. 10. Again, the unstable oscillations initially grow but then decrease to steady state, small-amplitude oscillations with frequency Ω_2, as shown in Fig. 11. This phenomenon can be interpreted in terms of the tangential motion time response of the contact subsystem, shown in Fig. 12. The velocity time history shows

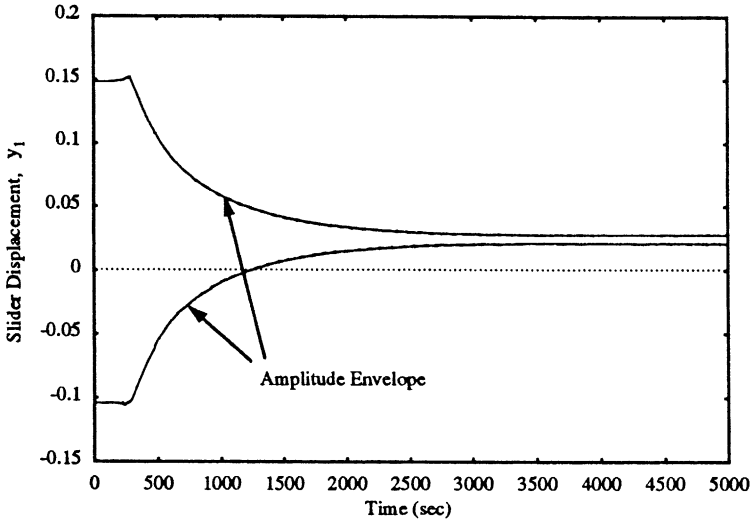

Fig. 10. The envelope of the slider time response for $\omega_o = 63.5$.

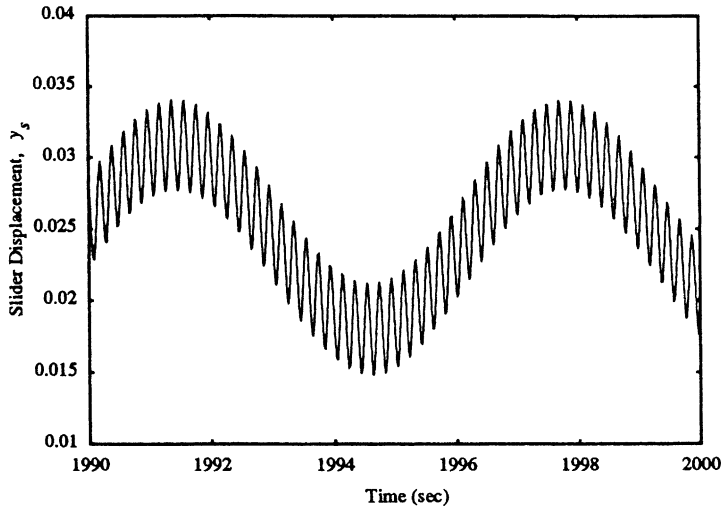

Fig. 11. A close-up of the slider time response for $\omega_o = 63.5$.

a locally unstable response growing with frequency Ω_2, as shown in the close-up of Fig. 13, here resulting in stick–slip oscillations. These steady state oscillations produce a forcing function on the slider of frequency Ω_2. Because the natural frequency of the slider is much lower ($\Omega_1 = 0.9950$) than the forcing frequency, the high frequency forcing function produces a high-frequency *low-amplitude* response. Indeed, the resonant response of the slider is of lower magnitude than the non-resonant response, although the smaller mass oscillates with large amplitudes in the resonant case.

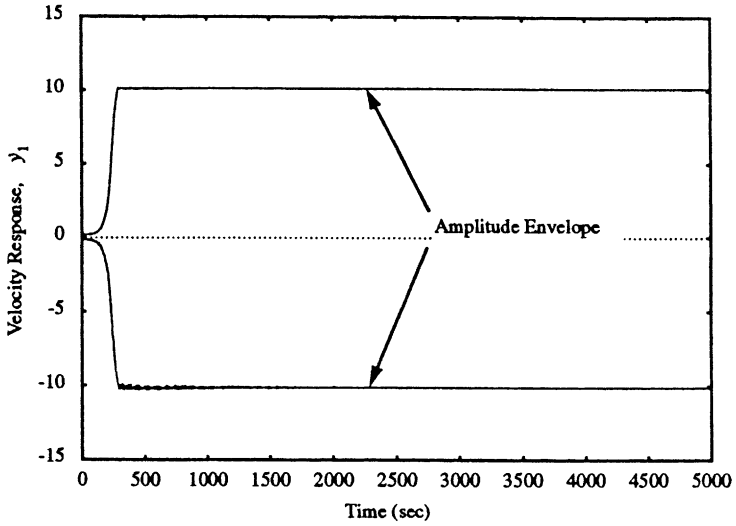

Fig. 12. The velocity response envelope for mass 1 for $\omega_o = 63.5$.

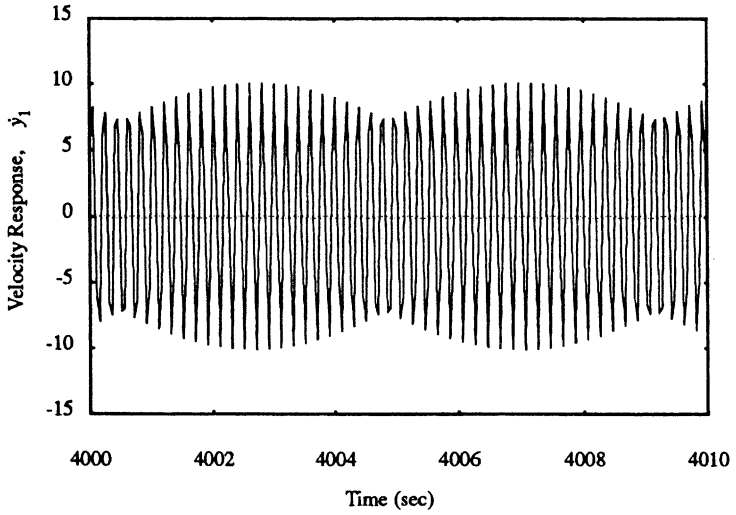

Fig. 13. A close-up of the velocity response of mass 1 for $\omega_o = 63.5$.

6. Conclusions

A general multi-d.o.f. model has been examined analytically for the existence of friction-related instabilities of the steady sliding position. Excited in the normal direction by a rough moving surface, and in the tangential direction by the non-linear coupling of friction, the system has been analyzed for resonance frequencies using first order averaging on the modal response equations of motion. Eigenvalue analysis of the averaged equations yielded stability criteria for the steady

sliding response. Numerical integration of the original system equations has verified the stability predictions.

The major conclusions of this work are as follows:

1. Friction-related sliding instabilities may arise in the multi-d.o.f. system with time-varying normal forces. While not friction-excited in the sense of the negative friction curve slope case, the unstable oscillations are friction-related because they originate from the interaction of the oscillatory normal force and the velocity-dependent friction coefficient. This *parametrically excited* instability is not possible for smooth contact; i.e., the case with constant normal force.
2. Non-linear friction laws (i.e., change in slope, or sticking at zero relative velocity) can bound locally unstable oscillations. In this case, the prescribed motion of sticking is the growth-limiting mechanism.

References

[1] D.M. Tolstoi, Significance of the normal degree of freedom and natural normal vibrations in contact friction, Wear 10 (1967) 199–213.
[2] D. Godfrey, Vibration reduced metal-to-metal contact and causes an apparent reduction in friction, ASLE Transactions 10 (1967) 183–192.
[3] B.V. Bundanov, V.A. Kudinov, D.M. Tolstoi, Interaction of friction and vibration, Soviet Journal of Friction and Wear 1 (1980) 79–89.
[4] J.R. Rice, A.L. Ruina, Stability of steady frictional slipping, Journal of Applied Mechanics 50 (1983) 343–349.
[5] D.P. Hess, A. Soom, Friction at lubricated line contact operating at oscillating sliding velocities, Journal of Tribology 112 (1990) 147–152.
[6] D.P. Hess, A. Soom, Unsteady friction in the presence of vibrations, in: I.L. Singer, H.M. Pollock (Eds.), Fundamentals of Friction: Macroscopic and Microscopic Processes, Kluwer Academic, Dordrecht, 1992, pp. 535–552.
[7] J.A. Greenwood, J. Williamson, Contact of nominally flat surfaces, Proceedings of the Royal Society. London A 295 (1966) 300–319.
[8] J.A.C. Martins, J.T. Oden, F.M.F. Simoes, A study of static and kinetic friction, International Journal of Engineering Science 28 (1990) 29–92.
[9] W.W. Tworzydlo, E.B. Becker, J.T. Oden, Numerical modeling of friction-induced vibration and dynamic instabilities, Applied Mechanics Reviews 47 (7) (1994) 255–274.
[10] S.W.E. Earles, C.K. Lee, Instabilities arising from the frictional interaction of a pin-disk system resulting in noise generation, Journal of Engineering for Industry 98 (1) (1976) 81–86.
[11] N.N. Krylov, N.N. Boguliubov, Introduction to Nonlinear Mechanics, Princeton University Press, Princeton, NJ, 1947.